A Time Domain Artificial Intelligence Radar System Using 33-GHz Direct Sampling for Hand Gesture Recognition

Jungwoon Park, Junyoung Jang, Geunhaeng Lee, Hyunmin Koh, Changhwan Kim, and Tae Wook Kim, *Senior Member, IEEE*

***Abstract*— This article introduces a time-domain-based artificial intelligence (AI) radar system for gesture recognition using 33-GS/s direct sampling technique. High-speed sampling using a time-extension method allows AI learning to be applied to a time-domain radar signal reflecting information on both dynamic and static gestures, and thus can recognize not only dynamic but also static gestures. The Vernier clock generators and high-speed active samplers applied with the time-extension technique makes sampling at 33 GS/s possible. A 1-D convolutional neural network and long short-term memory are employed for both static and dynamic gestures and recognition rates of 93.2% and 90.5% are obtained, respectively. The radar system is implemented using a 65-nm CMOS process with a power consumption of 95 mW.**

***Index Terms*— Artificial intelligence (AI) radar, gesture recognition, high-speed sampling, impulse radar ultra-wideband (IR-UWB), radar, sampler, time-to-digital converter (TDC), time-extension, transceiver, wireless sensing.**

I. Introduction

CONVENTIONAL radar systems have been used to detect the range, angle, and velocity of objects [1], [2]. However, recently, a learning-based radar system using artificial intelligence (AI) technology has emerged and has begun to be used for target recognition [3]. Such an advanced radar system can process significantly more information than a conventional radar approach and numerous studies are being conducted to enable its use in various applications. In particular, in [3]–[5], a new attempt at applying the AI radar to a hand-gesture recognition system is described.

In [3], an AI radar system for gesture recognition is implemented by applying machine learning to a conventional frequency-modulated continuous wave (FMCW) radar. There are three main phases during object recognition: a receiving step, a data processing step, and a recognition step. During the receiving process, a system board receives the reflected continuous wave from the target. The received signal includes the distinguishable Doppler shifts based on object movement. In addition, the differences in Doppler shift are visualized through the range-Doppler image (RDI) during the data processing stage [3]. Finally, during the recognition phase, the AI radar system learns and recognizes the features of the RDI generated according to the gesture movements.

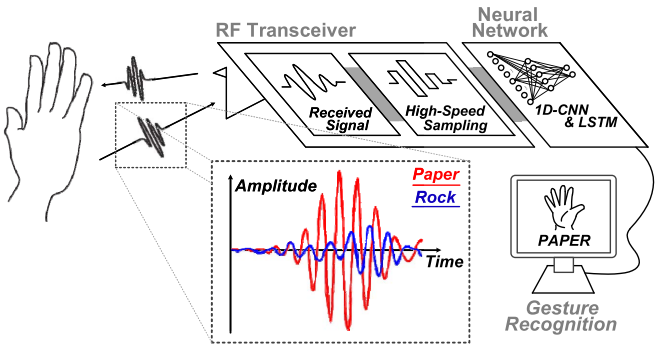

Fig. 1. Conceptual diagram of the proposed AI radar system applied in the time-domain.

However, the AI radar system described in [3] using the Doppler effect is difficult to recognize static gestures. (Because static gestures do not generate Doppler shifts.) By contrast, when analyzing signals by sampling at a high speed within the time domain, information including the position and the shape of the static gesture can be obtained. In addition, it is possible to recognize static gestures through a learning process. Moreover, if the system considers a series of static gestures as a single pattern, it can recognize even dynamic gestures. Therefore, in this article, a time-domain AI radar system that recognizes both static and dynamic gestures is proposed [6].

Fig. 1 shows a conceptual diagram of the proposed time-domain AI radar system. The impulse signals reflected from the target have different waveforms according to the position and shape of the target. This reflects the inherent characteristics of the gestures, as shown in the waveforms in Fig. 1. Gestures can be recognized by training a convolutional neural network (CNN) [7] or long short-term memory (LSTM) [8] with waveforms that include different characteristics of objects. The system can recognize an object even if there is no movement because the waveform analysis is conducted in the time domain without using the Doppler effect [9].

Manuscript received August 20, 2019; revised November 14, 2019 and January 6, 2020; accepted January 6, 2020. Date of publication January 30, 2020; date of current version March 26, 2020. This article was approved by Guest Editor Brian Ginsburg. This work was supported in part by the Institute of Information and Communications Technology Planning and Evaluation (IITP) Grant funded by the Korean Government (MSIT) under Grant 2017-0-00418 and in part by the IC Design Education Center (IDEC) for the CAD tool. *(Corresponding author: Tae Wook Kim.)*

The authors are with the School of Electrical and Electronic Engineering, Yonsei University, Seoul 03722, South Korea (e-mail: taewook.kim@yonsei.ac.kr).

Color versions of one or more of the figures in this article are available online at http://ieeexplore.ieee.org.

Digital Object Identifier 10.1109/JSSC.2020.2967547

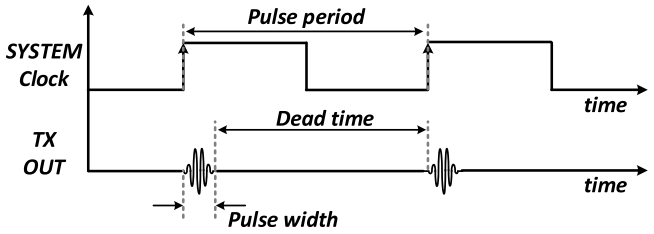

Fig. 2. Characteristics of the impulse signal.

In this article, an AI radar system is proposed that can process a high-speed signal with a low-speed analog-to-digital convertor (ADC) through the time-extension method to overcome the problem when using a high-speed ADC [11]. The time extension method is a technology utilizing the characteristics of the impulse signal used in the system. As shown in Fig. 2, the impulse signal has a dead time between impulse signals. The dead time refers to an interval in which no signal is transmitted between the impulse signal and the next impulse signal, which accounts for 99% of the entire period [12], [13]. The key idea of the time-extension method is to reduce the power consumption as much as possible by utilizing this dead time to feature the additional time. The high-speed signal is converted into a slow signal during the dead time. Forty samplers in the system sample the input signal at a high speed and store the charge in the holding capacitors. Next, during the dead time, the charges in each holding capacitor are transferred to the next stage sequentially according to the slow clock. This allows conversion of high-speed sampled signals into low-speed signals without loss of information. In practice, the proposed system samples a signal at 33 GS/s and converts it into a slow signal at 50 MHz. This enables processing the high-speed (4 GHz) signal even with a low-speed and low-power ADC [14]. Afterward, the AI radar learns and classifies waveforms using a 1-D-CNN and an LSTM algorithm optimized for waveform learning.

The remainder of this article is organized as follows. Section II introduces the proposed time-domain AI radar system with a block diagram and the timing diagram. Section III describes the circuit implementation and structure of the algorithm. Section IV details the measurement results. Finally, Section V summarizes this article and provides some concluding remarks.

II. Time-Domain AI Radar System

A. System Design

Fig. 3 shows the block diagram of the proposed system. TX transmits an impulse signal of 3–5 GHz within a period of 1 MHz [15], [16]. In addition, the signal that returned to the target is received by the receiver and is divided into two paths, a sampling path and a timing path. The sampling path is a path that samples the amplified input signal at a speed of 33 GS/s through the sample and holders and extends it to a 50-MHz signal. The timing path is a path that generates each clock for the high-speed sampling (= fast clock) and extension (= slow clock).

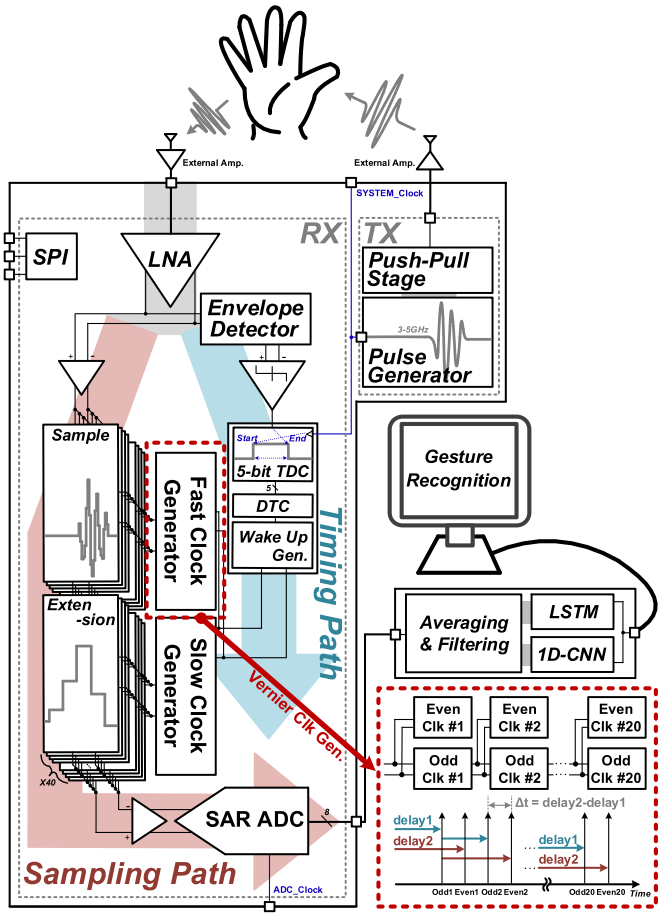

Fig. 3. Block diagram of the proposed AI radar system in the time domain.

The sampling path includes 40 samples and holders and extension switches. Each sample and holder store the charge in the holding capacitors according to the fast clock. In response to the slow clock, an extension switch converts the high-speed sampled signal into a low-speed signal based on the charge stored in the holding capacitors. After conversion into a slow signal of 50 MHz through the time-extension method, a low-speed ADC is used to digitize the signal.

The timing path includes an envelope detector and a comparator that reads the arrival time of the RX input, as well as a time-to-digital converter (TDC) that measures the time interval between the timing gap of the transmitted and received pulses [17]. Based on this time interval, the digital-to-time converter (DTC) determines the start times of the fast clock and the slow clock. In addition, to solve the problems of conventional clock generators, which have limitations with increasing the clock speed owing to a limited technology, a Vernier clock generator is used to secure a sampling rate of 33 GS/s. As shown in Fig. 3, the Vernier clock generator is composed of crossed odd and even clock generator cells. An alternating clock timing can be generated to achieve up to twice the clock speed of a conventional clock generator.

The signal sampled within the time domain is converted into a digital signal through a low-speed ADC. The digital information obtained by the ADC is then preprocessed in a suitable form for the algorithm. Because the waveform is made

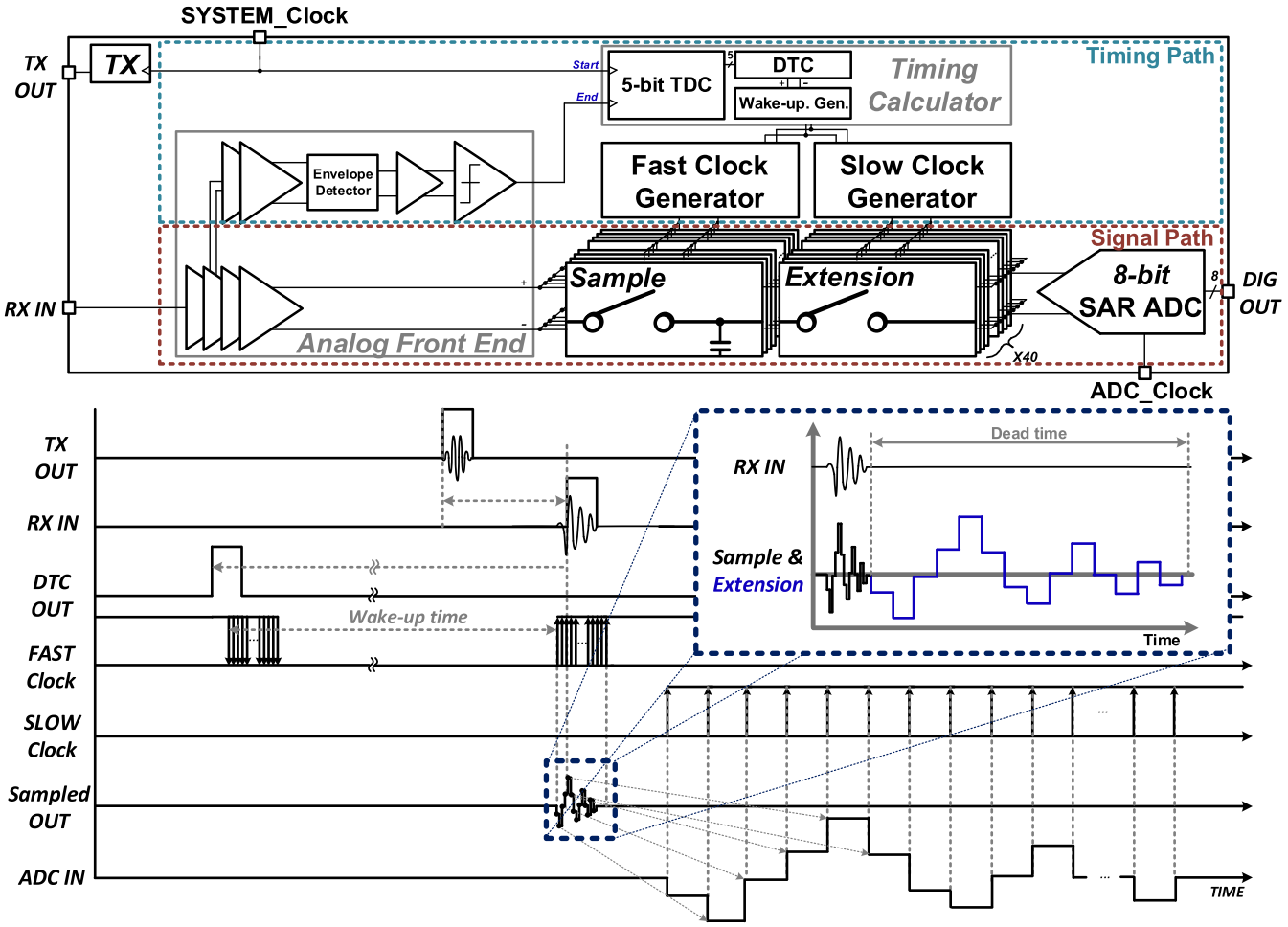

Fig. 4. Timing diagram of the proposed time-domain-based AI radar system.

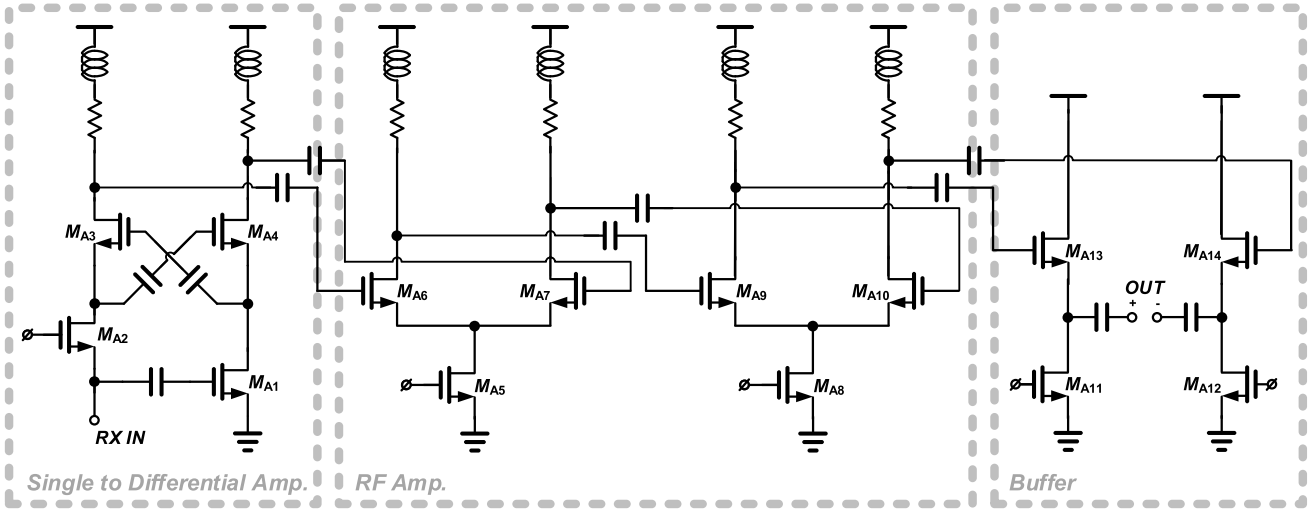

Fig. 5. Schematic of the analog front end.

up of 1-D data, the characteristics of the waveform are learned using a 1-D-CNN for static gestures. In addition, the dynamic gesture is learned using the LSTM. Thus, both static and dynamic gestures can be recognized through the proposed AI radar system.

B. Timing Diagram

Fig. 4 shows the timing diagram of the time-domain-based AI radar system. The timing path contains an envelope detector, a comparator, a timing calculator, and fast and slow clock generators. The sampling path contains LNAs, 40 sample

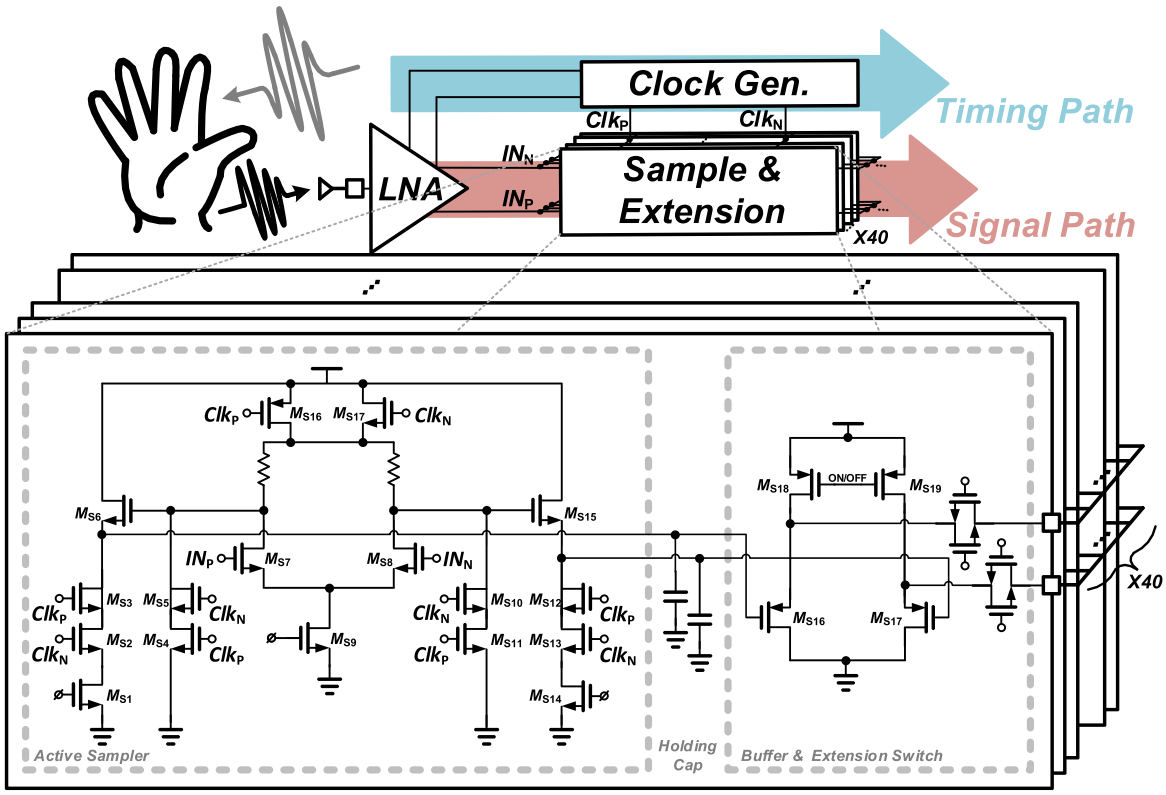

Fig. 6. Circuit diagram of the sample and extension blocks.

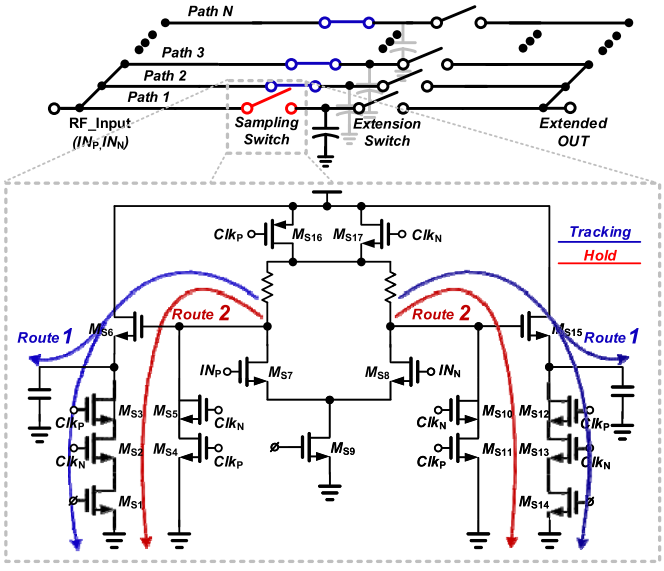

Fig. 7. Circuit diagram of the sampler.

and extension blocks, and an ADC. The timing calculator consists of a TDC, a DTC, and a wake-up time generator. First, TX and RX are synchronized based on the same clock (SYSTEM_Clock). As mentioned earlier, the TDC in the timing path measures the time interval between TX OUT and RX IN. This allows the system to know how much time has passed since the signal was sent. In addition, the system only recognizes the signal from the nearest target using a leading-edge detection method because it focuses on hand gesture recognition. The leading-edge detection method detects only the first arriving signal and ignores the following signals [18]. The start times of the fast and slow clocks are determined based on the timing calculator when considering the timing gap measured by the TDC and the wake-up time.

The wake-up time is the time taken to turn on the sampler. The system includes an active sampler for a high-speed sampling operation, and the system is turned off for most of the time to save the power consumption of the system by utilizing the characteristics of the impulse signal [10], [11]. The sampler works instantly according to the fast clock only when the signal arrives. In other words, it is necessary to turn on the active sampler in advance and then conduct the sample according to the arrival time of the input signal. The time taken for the sampler to recover to a stable dc point is called the wake-up time. Thus, if the signal arrives during the Nth period, it can be understood that the actual sampling is applied from the $(N+1)$th period. In addition, the period of the system clock is 1 μs, which is sufficiently long compared with the retrigger time of the comparator, and thus the system can prepare for the sampling regardless of the trigger time. Afterward, 40 samplers operate by the fast and slow clocks generated by the timing calculator and convert the high-speed signal into a low-speed signal.

III. System Implementation

A. Circuit Implementation

Fig. 5 shows a circuit diagram of the LNA and the buffer at the beginning of the sampling path. A single to differential LNA is designed to receive wideband signals and utilizes

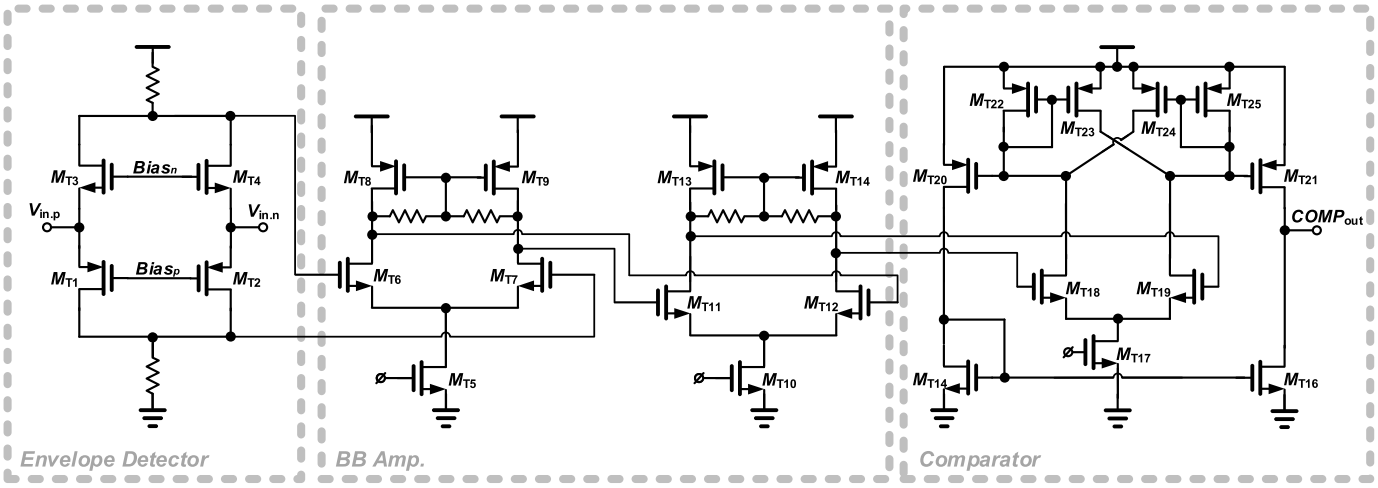

Fig. 8. Schematic of the envelop detector, baseband amplifier, and comparator.

TABLE I
POWER DISSIPATION SUMMARY OF THE SYSTEM

Block	Power consumption
RF Amplifier	4 mW
Buffer	9 mW
Envelope detector	0.1 mW
Baseband amplifier	9.5 mW
Comparator	18 mW
Sampler	0.18 mW (dynamic)

a cross-coupled capacitor. The gain is 12.6 dB with 4-mA current and the bandwidth is 9 GHz. Because the buffer should drive 40 samplers, it has heavy loading. Thus, a bandwidth extension technique such as shunt peaking is utilized in the amplifiers [19]. The total analog front-end gain is 22.4 dB and the bandwidth is 9 GHz, consuming 42 mA.

The amplified input signal enters the 40 samplers simultaneously in parallel. Fig. 6 shows the circuit diagram of the 40 sample and extension blocks. Each block consists of three parts, namely a sample and a holder, a buffer, and an extension switch. Depending on the fast clock, each sample and holder store the charges in a holding capacitor sequentially. The holding capacitor is 581 fF. The extension switch then transfers the stored charges from each holding capacitor to the next stage in time with the slow clock. This allows a high-speed signal to be converted into a slow signal of 50 MHz.

Fig. 7 shows a schematic and detailed operation of the active sampler. Normally, the source follower (M_{S6} and M_{S15}) is on and tracks the input signal. After tracking, the source follower is turned off according to the fast clock and activates route 2. At the same time, the charges stored in the holding capacitor along route 1 continue to hold. Along each route, a charge cancellation method using dummy capacitors (M_{S3}, M_{S5}, M_{S10}, and M_{S12}) is applied to prevent a charge injection [20]. Therefore, the dummy capacitors use half the size of the ON/OFF switch (M_{S2}, M_{S4}, M_{S11}, and M_{S13}). When the sampler of path 1 finishes its operation, the sampler of path 2 operates in succession and the operation continues up to path N, where $N = 40$. Each sampler runs once per SYSTEM_Clock, but the difference in the operating time between each sampler is 30 ps, which achieves a 33-GS/s sampling rate.

The fast and slow clocks running the sample and holders are generated along the timing path. Fig. 8 shows a schematic of the envelope detector [21] and comparator [22] on this path, which is the front of the timing calculator shown in Fig. 4. An envelope detector generates a digital pulse based on the timing of the input signal. The baseband amplifier amplifies the digital pulse with a 26-dB gain. The comparator extracts the leading edge of the input signal based on the threshold voltage (V_{th}). If V_{th} is too high, the sensitivity of the receiver will be reduced, and if V_{th} is too low, the system will become extremely vulnerable to noise. Here, V_{th} was set to the 400-mV level.

The timing path used in this system applies an energy detection method to obtain the timing information of the input signal and determine the timing of the sampling. In most cases, the energy detection method has poor sensitivity. Thus, the SNR performance of the sampling path is better than that of the timing path, which uses an energy detection method. If the system targets a short operating distance, the energy detection method will not incur a problem in terms of sensitivity. However, a system that shows better sensitivity, such as a correlator-based receiver, will be useful for increasing the operation distance [23]. Fig. 9 shows the block and timing diagrams of the Vernier clock generator. Two types of delay blocks (odd and even cells) intersect to create a faster clock. This can produce a delay as small as $\Delta t = \text{delay1} - \text{delay2}$. Moreover, Δt is directly related to the sampling speed. In addition, because each delay block is adjustable, the sampling speed can be controlled as desired. The Vernier clock generator in the system generates a 30-ps delay, which enables a 33-GS/s sampling rate.

Fig. 10 shows the simulation results of the sample and extension process. As Fig. 10 indicates, the sampling process

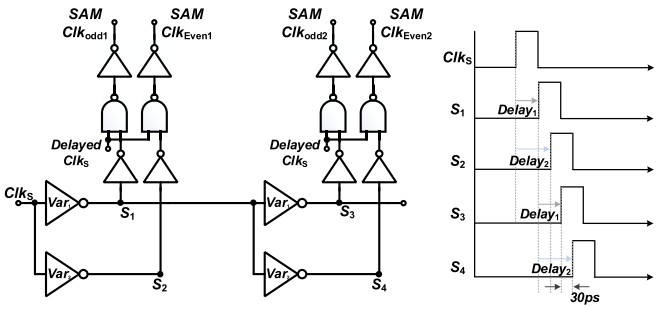

Fig. 9. Block diagram of the Vernier clock generator.

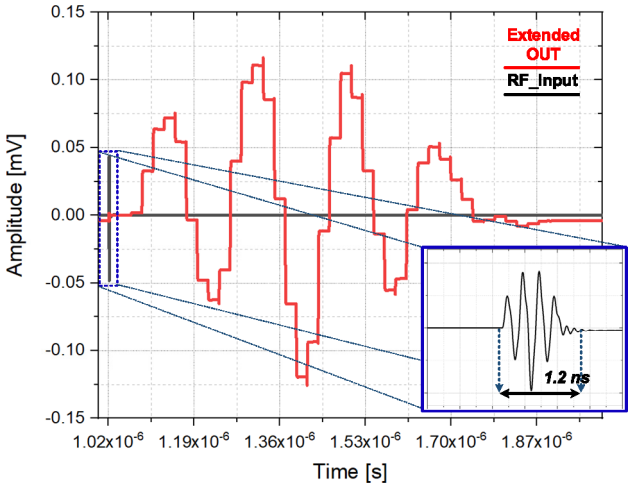

Fig. 10. Simulation result of sample and extension.

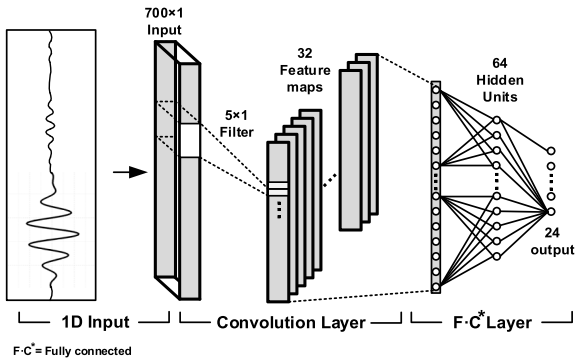

Fig. 11. Structure of 1-D-CNN.

is conducted for approximately 1.2 ns starting from the first clock time to the 40th clock time. The received signal in this sampling section is sampled at 33 GS/s and then extended to a low-speed signal. The power consumption of each block is summarized in Table I.

B. Algorithm Structure

Figs. 11 and 12 show the structure of this system with a neural network, a 1-D-CNN, and the LSTM algorithm. As mentioned earlier, the signal within the time domain is a 1-D signal and the algorithm structure is designed to process a 1-D signal. The CNN model uses a convolution layer and a

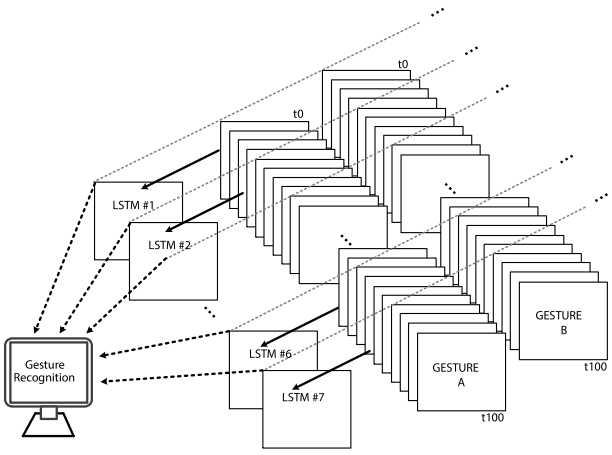

Fig. 12. Structure of LSTM.

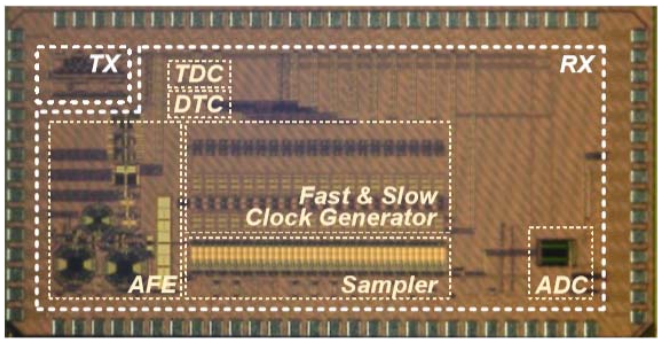

Fig. 13. Die microphotography of the transceiver.

fully connected layer, not including a pooling process. A total of 32 feature maps were used and the last hidden layer was composed of three dimensions. Because both the timing path and the sampling path have sufficient margins to recognize gestures, the greatest impact on the recognition rate comes from the algorithm. The number of feature maps and the size of the filter were determined after several optimizations of the collected static gesture data.

A dynamic gesture can be understood as a series of static gestures. That is, to characterize dynamic gestures, the system detects the changes in waveform for several seconds. It is therefore necessary to set the proper frame rate such that the features of the dynamic gestures will not be lost. The system is configured to run at a speed of approximately 50 fps, which is sufficient to catch the features of the gestures.

Dynamic gestures are recognized using the LSTM algorithm, through which future static gestures can be predicted using the previous and current static gestures. This allows recognizing a series of static gestures as a single dynamic gesture. A single dynamic gesture consists of 100 consecutive static gesture waveforms. A total of 100 waveform data listed in chronological order are converted into a single sample with 14 time-steps. To clearly classify the features for each operation and increase the efficiency of the computation, the LSTM algorithm was implemented in parallel, as shown in Fig. 12.

TABLE II
PERFORMANCE SUMMARY TABLE

	This Work	[3], [4]	[24]	[25]
Technology	**65nm CMOS**	0.35um SiGe	0.13um SiGe	-
Channel	**1TX 1RX**	2TX 4RX	1TX 1RX	1TX 4RX
Feature	**Pulse radar**	FMCW radar	Pulse radar	FMCW radar
System Frequency	**3~5 GHz**	57~64 GHz	94 GHz	24.8 GHz
Power Consumption	**95 mW**	990 mW	1900 mW	-
Sampling Speed	**33 GS/s**	N/A	N/A	N/A
Measurement Distance	**50 cm**	30 cm	-	50 cm
# of gesture can classify	**Static gesture : 5** **Dynamic gesture : 6**	Static gesture : 0 Dynamic gesture : 10	-	Static gesture : 0 Dynamic gesture : 7
Average recognition rate	**93.2 % / 90.5 %**	87 %	-	83.33 %
Size	**3 x 1.5 mm^2**	4.5 x 4.5 mm^2	4.4 x 1.4 mm^2	Bench top

TABLE III
ACCURACY OF HAND GESTURE RECOGNITION

Method	*Average Accuracy	Static Gesture				
		A	B	V	D	L
1D-CNN	**93.2%**	93.2%	96.6%	93.2%	89.8%	93.2%

Method	*Average Accuracy	Dynamic Gesture					
		Opening	Clenching	Forward	Backward	Swing	Pointing
LSTM	**90.5%**	97%	86%	93%	96%	87%	84%

* Average accuracy of hand gesture recognition

IV. MEASUREMENT RESULTS

The proposed time-domain AI radar system is implemented by a 65-nm CMOS process. Fig. 13 shows a micro-photograph of the transceiver chip, with a size of 4.5 mm^2. The power consumptions of the transmitter and the receiver are 2.3 and 90.2 mW, respectively, whose ADC consumes only 2.5 mW.

Fig. 14 shows the measurement setup applied. The measurement distance was 30–50 cm. A Vivaldi antenna was used to minimize the influence of the signal going along the direct path between the transmitter and the receiver, the gain of which is 6 dBi. The transmitter utilizes Gaussian shaping to generate a 3–5-GHz impulse signal [26]. In addition, a high-pass filter (Mini-Circuits VHF-3100 +) is used to reduce the effect of narrowband interference in a wireless environment.

As shown in Fig. 15, the time-domain based AI radar system receives the signal returned from the target and generates an 8-bit digital signal as output. The final 8 bits of digital output are sent to the PC through a logic analyzer. Then, they go through an averaging and low pass filtering process before being applied to the 1-D-CNN and LSTM. As shown in the graph, signals have different characteristics depending on the shape of the gesture.

As shown in Fig. 16, five static and six dynamic gestures were selected for verification, namely making "A," "B," "V," "D," and "L" letters in the American sign language [27] for signaling "opening," "clenching," "forward," "backward," "swing," and "pointing," respectively. A total of 10 000 static gesture data were divided into ten subsets, with 1000 gestures each. The subsets were then separated into training and validation sets prior to use. In the case of a dynamic gesture, 30 000 data were collected and divided into ten subsets using the same method. A tenfold cross-validation was adopted during the training phase [28], and for verifying the recognition rate, the gestures of ten different people were used during the test phase. The 1-D-CNN and LSTM algorithms were applied in this system.

Fig. 17 shows the measured waveforms of static gestures. The "A," "B," and "V" motions, which have significant differences in shape, reflect the unique characteristics of each gesture. In addition, the arrival time and amplitude of the waveform generally contain information regarding the position and distance of the gesture. The minimum performance of the ADC, which can distinguish the five static gestures mentioned above, was 6 bits, and the ADC and the sampler were designed with a margin of 8 bits. Owing to the use of sufficient margins, the system was shown to be robust to jitters and variations in the PVT. In addition, if the system learns the waveform itself including a distortion during the learning stage, even if a distortion occurs, the average recognition rate will not decrease.

Fig. 18 shows a waveform of a dynamic gesture in the time domain. A dynamic gesture can be understood as a series of static gestures. In the case of a clenching gesture, the process

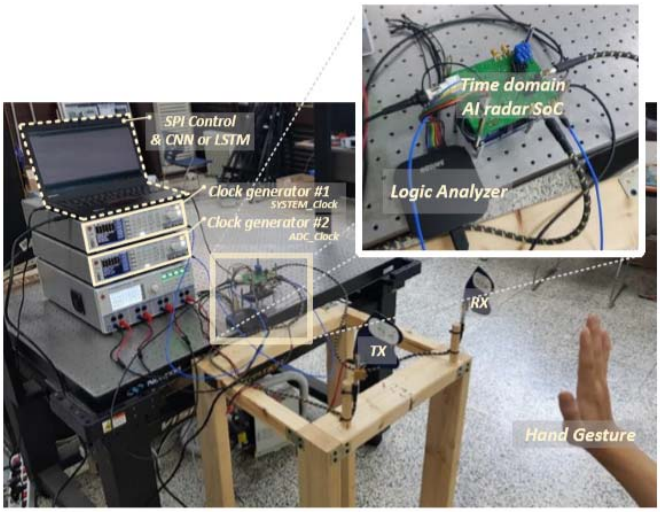

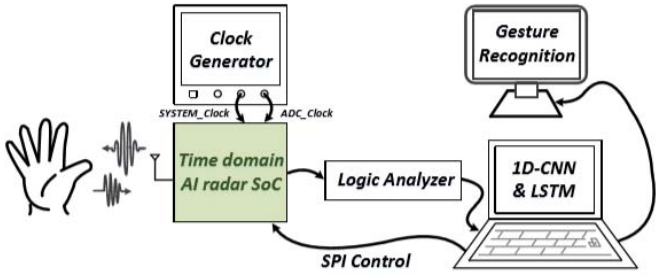

Fig. 14. Measurement Environment.

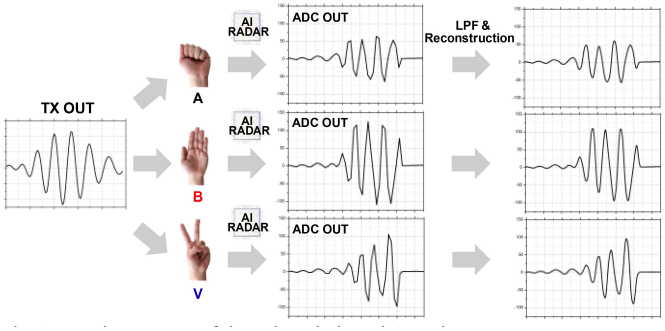

Fig. 15. Entire process of time-domain-based AI radar system.

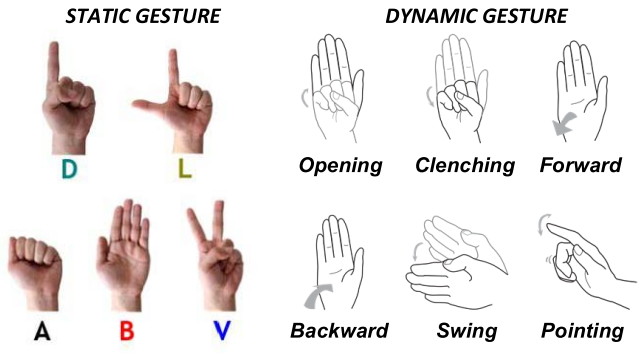

Fig. 16. Static and dynamic gestures recognized during gesture evaluation.

can be seen as starting with the waveform graph shown in B and changing to the graph in A. Even for the "pointing" motion in which the information about the reflecting surface is complicated; the motion of the angle is slightly changed.

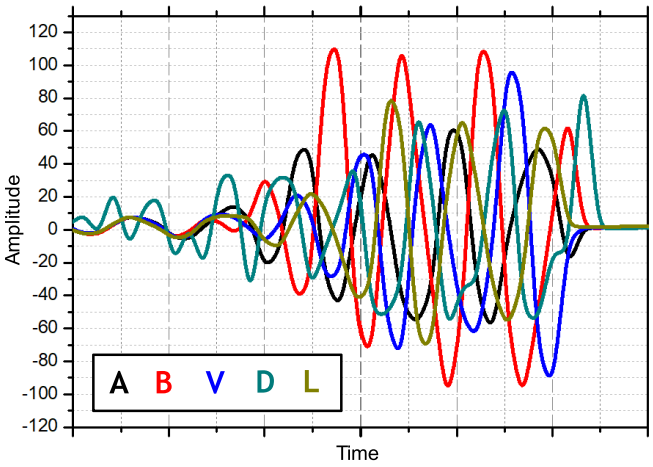

Fig. 17. Measurement results of static gesture.

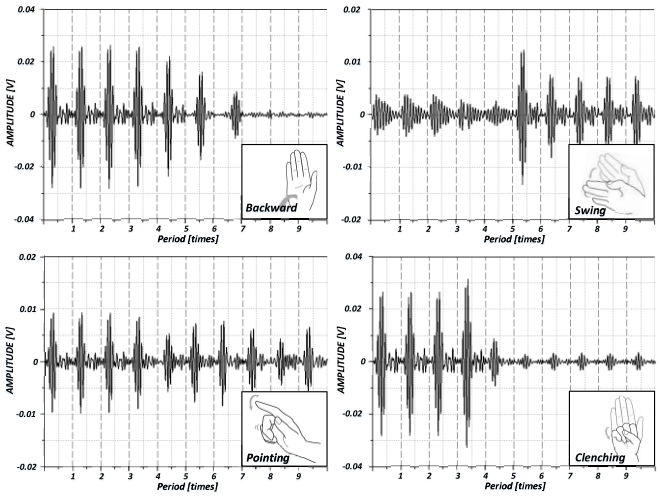

Fig. 18. Measurement results of dynamic gesture.

TABLE IV
CONFUSION MATRIX OF STATIC GESTURE RECOGNITION

Static Gestures	A	B	V	D	L
A	93.2 %	3.4 %	0 %	0 %	3.4 %
B	0 %	96.6 %	3.4 %	0 %	0 %
V	0 %	3.4 %	93.2 %	0 %	3.4 %
D	0 %	6.8 %	0 %	89.8 %	3.4 %
L	0 %	3.4 %	3.4 %	0 %	93.2 %

Table II shows the performance of the time-domain based AI radar system. The proposed radar system is based on a pulse radar system and achieves a sampling speed of 33 GS/s. The power consumption is 95 mW at a 1-V supply voltage. The average recognition rates of the static and dynamic gestures were 93.2% and 90.5%, respectively, thereby overcoming the limitations of a previous AI radar system, which only focused on dynamic gestures. The recognition rates for each gesture are listed in Table III. Tables IV and V show the confusion matrixes of static and dynamic gestures, respectively.

TABLE V
CONFUSION MATRIX OF DYNAMIC GESTURE RECOGNITION

Dynamic Gestures	Opening	Clenching	Forward	Backward	Swing	Pointing
Opening	97 %	2 %	0 %	0 %	0 %	1 %
Clenching	7 %	86 %	0 %	0 %	6 %	1 %
Forward	2%	0 %	93 %	2%	3%	0 %
Backward	0 %	3 %	0 %	96 %	0 %	1 %
Swing	1 %	0 %	3 %	1 %	87 %	8 %
Pointing	2%	4 %	0 %	4 %	6 %	84 %

V. CONCLUSION

In this article, a time-domain based AI radar system using direct sampling at 33 GS/s is proposed. This system can recognize both static and dynamic gestures by learning the characteristics of the waveform returning from the target. High-speed sampling was processed using a Vernier clock generator and an active sampler structure. In addition, the high-speed sampled signal was converted into a low-speed signal through a time-extension method such that digital data can be generated using a low-speed, low-power ADC. By applying 1-D-CNN and LSTM, recognition rates of 93.2% and 90.5% were recorded for five types of static gestures and six types of dynamic gestures, respectively.

ACKNOWLEDGMENT

The authors would like to thank Rohde and Schwarz for their support of the test instruments applied.

REFERENCES

[1] G. Ossberger, T. Buchegger, E. Schimback, A. Stelzer, and R. Weigel, "Non-invasive respiratory movement detection and monitoring of hidden humans using ultra wideband pulse radar," in *Proc. Int. Workshop Ultra Wideband Syst. Joint Conf. Ultra Wideband Syst. Technol.*, Kyoto, Japan, Sep. 2004, pp. 395–399.

[2] J. Lee, Y.-A. Li, M.-H. Hung, and S.-J. Huang, "A fully-integrated 77-GHz FMCW radar transceiver in 65-nm CMOS technology," *IEEE J. Solid-State Circuits*, vol. 45, no. 12, pp. 2746–2756, Dec. 2010.

[3] J. Lien, "Soli: Ubiquitous gesture sensing with millimeter wave radar," *ACM Trans. Graph.*, vol. 35, p. 142, Jul. 2016.

[4] I. Nasr *et al.*, "A highly integrated 60 GHz 6-channel transceiver with antenna in package for smart sensing and short-range communications," *IEEE J. Solid-State Circuits*, vol. 51, no. 9, pp. 2066–2076, Sep. 2016.

[5] S. Wang, J. Song, J. Lien, I. Poupyrev, and O. Hilliges, "Interacting with soli: Exploring fine-grained dynamic gesture recognition in the radio-frequency spectrum," in *Proc. 29th Annu. Symp. User Interface Softw. Technol. (UIST)*, 2016, pp. 851–860.

[6] J. Park, J. Jang, G. Lee, H. Koh, C. Kim, and T. W. Kim, "A time domain artificial intelligence radar for hand gesture recognition using 33-GHz direct sampling," in *Proc. Symp. VLSI Circuits*, Jun. 2019, pp. 24–25.

[7] Y. LeCun, "Convolutional networks for images, speech, and time series," *The Handbook of Brain Theory and Neural Networks*. VP and Chief AI Scientist, 1995. [Online]. Available: http://yann.lecun.com/

[8] S. Hochreiter and J. Schmidhuber, "Long short-term memory," *Neural Comput.*, vol. 9, pp. 1735–1780, Nov. 1997.

[9] S. Y. Kim, H. G. Han, J. W. Kim, S. Lee, and T. W. Kim, "A hand gesture recognition sensor using reflected impulses," *IEEE Sensors J.*, vol. 17, no. 10, pp. 2975–2976, May 2017.

[10] H. Landau, "Sampling, data transmission, and the Nyquist rate," *Proc. IEEE*, vol. 55, no. 10, pp. 1701–1706, Oct. 1967.

[11] H. G. Han, B. G. Yu, and T. W. Kim, "A 1.9-mm-Precision 20-GHz direct-sampling receiver using time-extension method for indoor localization," *IEEE J. Solid-State Circuits*, vol. 52, no. 6, pp. 1509–1520, Jun. 2017.

[12] S. Geng, D. Liu, Y. Li, H. Zhuo, W. Rhee, and Z. Wang, "A 13.3 mW 500 Mb/s IR-UWB transceiver with link margin enhancement technique for meter-range communications," *IEEE J. Solid-State Circuits*, vol. 50, no. 3, pp. 669–678, Mar. 2015.

[13] M. Crepaldi, C. Li, J. R. Fernandes, and P. R. Kinget, "An ultra-wideband impulse-radio transceiver chipset using synchronized-OOK modulation," *IEEE J. Solid-State Circuits*, vol. 46, no. 10, pp. 2284–2299, Oct. 2011.

[14] P. J. A. Harpe *et al.*, "A 26 μW 8 bit 10 MS/s asynchronous SAR ADC for Low Energy Radios," *IEEE J. Solid-State Circuits*, vol. 46, no. 7, pp. 1585–1595, Jul. 2011.

[15] V. V. Kulkarni, M. Muqsith, K. Niitsu, H. Ishikuro, and T. Kuroda, "A 750 Mb/s, 12 pJ/b, 6-to-10 GHz CMOS IR-UWB transmitter with embedded on-chip antenna," *IEEE J. Solid-State Circuits*, vol. 44, no. 2, pp. 394–403, Feb. 2009.

[16] P. P. Mercier, D. C. Daly, and A. P. Chandrakasan, "An energy-efficient all-digital UWB transmitter employing dual capacitively-coupled pulse-shaping drivers," *IEEE J. Solid-State Circuits*, vol. 44, no. 6, pp. 1679–1688, Jun. 2009.

[17] T. Rahkonen and J. Kostamovaara, "The use of stabilized CMOS delay lines for the digitization of short time intervals," *IEEE J. Solid-State Circuits*, vol. 28, no. 8, pp. 887–894, Aug. 1993.

[18] G. Lee, J. Park, J. Jang, T. Jung, and T. W. Kim, "An IR-UWB CMOS transceiver for high-data-rate, low-power, and short-range communication," *IEEE J. Solid-State Circuits*, vol. 54, no. 8, pp. 2163–2174, Aug. 2019.

[19] S. Mohan, M. Hershenson, S. Boyd, and T. Lee, "Bandwidth extension in CMOS with optimized on-chip inductors," *IEEE J. Solid-State Circuits*, vol. 35, no. 3, pp. 346–355, Mar. 2000.

[20] C. Eichenberger and W. Guggenbuhl, "Dummy transistor compensation of analog MOS switches," *IEEE J. Solid-State Circuits*, vol. 24, no. 4, pp. 1143–1146, Aug. 1989.

[21] B. Van Liempd *et al.*, "A 3 μW fully-differential RF envelope detector for ultra-low power receiver," in *Proc. IEEE Int. Symp. Circuits Syst.*, May 2012, pp. 1496–1499.

[22] X. Qian and T. H. Teo, "A low-power comparator with programmable hysteresis level for blood pressure peak detection," in *Proc. IEEE Region Conf.*, Nov. 2009, pp. 1–4.

[23] B. Schleicher, I. Nasr, A. Trasser, and H. Schumacher, "IR-UWB radar demonstrator for ultra-fine movement detection and vital-sign monitoring," *IEEE Trans. Microw. Theory Techn.*, vol. 61, no. 5, pp. 2076–2085, May 2013.

[24] A. Arbabian, S. Callender, S. Kang, M. Rangwala, and A. M. Niknejad, "A 94 GHz mm-Wave-to-baseband pulsed-radar transceiver with applications in imaging and gesture recognition," *IEEE J. Solid-State Circuits*, vol. 48, no. 4, pp. 1055–1071, Apr. 2013.

[25] S.-J. Ryu, J.-S. Suh, S.-H. Baek, S. Hong, and J.-H. Kim, "Feature-based hand gesture recognition using an FMCW radar and its temporal feature analysis," *IEEE Sensors J.*, vol. 18, no. 18, pp. 7593–7602, Sep. 2018.

[26] R. Xu, Y. Jin, and C. Nguyen, "Power-efficient switching-based CMOS UWB transmitters for UWB communications and Radar systems," *IEEE Trans. Microw. Theory Techn.*, vol. 54, no. 8, pp. 3271–3277, Aug. 2006.

[27] C. Valli and C. Lucas, *Linguistics of American Sign Language: An Introduction*. Washington, DC, USA: Gallaudet Univ. Press, 2000.

[28] R. Kohavi, "A study of cross-validation and bootstrap for accuracy estimation and model selection," *Int. Joint Artif. Intell.*, vol. 14, no. 2, pp. 1137–1145, 1995.

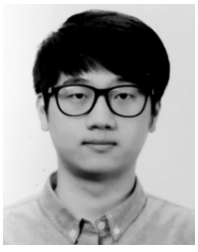

Jungwoon Park was born in Seoul, South Korea, in 1992. He received the B.S. degree in electrical and electronic engineering from Yonsei University, Seoul, in 2015, where is currently pursuing the Ph.D. degree.

His research interests are communication system for Internet of Things, RF system, and time domain artificial intelligence (AI) radar system for hand gesture recognition.

Junyoung Jang was born in South Korea in 1990. He received the B.S. degree in electronics engineering from Yonsei University, Seoul, South Korea, in 2014, where he is currently pursuing the Ph.D. degree in electrical and electronic engineering.

His research interest includes RF/analog circuit and systems for wireless application.

Geunhaeng Lee was born in Seoul, South Korea, in 1991. He received the B.S. degree in electronic and electrical engineering from Dankook University, Yongin-si, South Korea, in 2014. He is currently pursuing the Ph.D. degree with Yonsei University, Seoul.

His research interests are RF amplifiers, mixed-signal circuits, and circuits and systems for wireless communication.

Hyunmin Koh received the B.S. and M.S. degrees in electrical engineering from Yonsei University, Seoul, South Korea, in 2017 and 2019, respectively.

His current research interests include stacked DRAM, such as HBM.

Changhwan Kim was born in Seoul, South Korea, in 1994. He received the B.S. degree in electrical and electronic engineering from Yonsei University, Seoul, in 2019.

His research interests are communication system for Internet of Things and RF system.

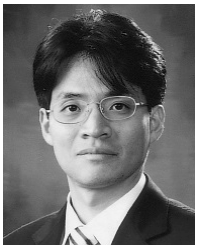

Tae Wook Kim (Senior Member, IEEE) was born in Seoul, South Korea, in 1974. He received the B.S. degree in electrical engineering from Yonsei University, Seoul, in 2000, and the M.S. and Ph.D. degrees from the Korea Advanced Institute of Science and Technology (KAIST), Daejeon, South Korea, in 2002 and 2005, respectively.

From July 2002 to December 2005, he was with Integrant Technology, Inc. From January 2006 to July 2007, he was with Qualcomm, Inc., Austin, TX, USA, where he was involved with DVB-H and Media FLO chip design. Since September 2007, he has been with the School of Electrical and Electronic Engineering, Yonsei University, where he is currently a Professor. His research interests are in microwave, RF, analog, and mixed-signal ICs and systems.

Dr. Kim was an Organizing Committee Member of the IEEE A-SSCC 2011 and the IEEE MWSCAS 2011. He serves as a Technical Program Committee Member for the IEEE ISSCC, the IEEE APMC, and the IEEE A-SSCC, and a Steering Committee Member for the IEEE MWSCAS.